ELSEVIER

J. Non-Newtonian Fluid Mech., 80 (1999) 93–113

Journal of Non-Newtonian Fluid Mechanics

# Understanding thixotropic and antithixotropic behavior of viscoelastic micellar solutions and liquid crystalline dispersions. I. The model

F. Bautista [a], J.M. de Santos [a], J.E. Puig [a], O. Manero [b,*]

[a] *Departamento de Ingeniería Química, Universidad de Guadalajara, Boul. M. García Barragán 1451, Guadalajara, Jal. 44430, Mexico*

[b] *Instituto de Investigaciones en Materiales, Universidad Nacional Autónoma de México, Apdo. Postal 70-360, Mexico D.F. 04510, Mexico*

Received 11 August 1997; received in revised form 16 March 1998

**Abstract**

A simple model consisting of the Upper Convected Maxwell constitutive equation and a kinetic equation for destruction and construction of structure, first proposed by Fredrickson in 1970, is used here to reproduce the complex rheological behavior of viscoelastic systems that also exhibit thixotropy and rheopexy under shear flow. The model requires five parameters that have physical significance and that can be estimated from rheological measurements. Several steady and unsteady flow situations were analyzed with the model. The model predicts creep behavior, stress relaxation and the presence of thixotropic loops when the sample is subjected to transient stress cycles. Such behavior has been observed with surfactant-based solutions and dispersions. The role of the characteristic time for structure built up, $\lambda$, in the extent and shape of the thixotropic loops is demonstrated. 

*Keywords:* Thixotropy; Viscoelasticity; Micellar solutions

## 1. Introduction

Concentrated suspensions, solutions of polyelectrolytes, biological and other complex fluids are known to exhibit thixotropy, antithixotropy (rheopexy) and other complex rheological behavior [1–5]. Recent experimental reports [6–10] have shown that elongated micellar solutions, dispersions of liquid crystals and lamellar liquid crystalline phases exhibit time-dependent rheological behavior and viscoelasticity. However, very few studies have been devoted to the analysis of thixotropic phenomena in liquid crystals and micellar solutions [11,12].

* Corresponding author. Fax: + 52 5 6161201.

0377-0257/99/$ - see front matter 
*PII* S0377-0257(98)00081-0

In the analysis of thixotropic phenomena, two approaches can be distinguished [5]: a continuum mechanics one, which is phenomenological in nature, and another based in the understanding of the basic processes leading to structural changes as the sample is deformed. In the latter approach, it is usually considered that the instantaneous rheological properties depend on a structural parameter (i.e. molecular entanglements, network junctions, liquid crystalline microdomains, etc.) that is changing with deformation history. Thus, the rheological functions, such as viscosity, depend on the actual level of the fluid structure. When the structure breaks down due to flow, viscosity consequently decreases. Mewis [13], in his review article, points out that the non-linear, time-dependent behavior of the rheological functions is caused by changes in the internal structure of the material, which can be described by a set of two equations. One is a constitutive equation that gives the instantaneous stress $\tau$ as a function of the instantaneous kinematics $D(r, t)$ for every possible state of the structure at any position, $r$. The other is a kinetic equation that describes the rate of change of the degree of structure $s(r, t)$ with the instantaneous kinematics, i.e. the imposed shear rate, $\dot{\gamma}$.

Due to the kinetics of structure breakdown and reformation usually being system-dependent, a unique kinetic expression for these processes is not possible. Thus, several models have been proposed which assign different forms to the basic constitutive equation and to the kinetic equation for the structural parameter. Usually, the structural parameter, which has to be obtained from experimental data, is related to a measurable rheological property. The apparent shear viscosity ($\eta$) has been used as a measure of structure [13,14]. This is equivalent to assume that the viscosity is proportional to the instantaneous number of structural points, $N(t)$ (i.e. bonds, links or entanglements). In this approach, it is usually considered that the rate of change of the number of structural points depends on their instantaneous number and on the work done on the system [15–19]. Some time ago, Fredrickson [20] proposed a simple kinetic equation for the destruction and construction of structure coupled to a Newtonian constitutive equation with a time dependent viscosity to predict the thixotropic behavior of inelastic suspensions under shear flow. This model can predict Non-Newtonian behavior and apparent yield stresses (Bingham plastic-like behavior) in steady shear-flow and thixotropic loops under time dependent shear histories. The kinetic equation of Fredrickson has the following form [20]:

$$\frac{\mathrm{d}\varphi}{\mathrm{d}t} = \frac{(\varphi_0 - \varphi)}{\lambda} + k(\varphi_\infty - \varphi)\tau{:}D. \tag{1}$$

Here, $\varphi$ is the fluidity ($\equiv \eta^{-1}$), $\varphi_0$ and $\varphi_\infty$ are the fluidities at zero and very high shear rates, respectively, $\lambda$ is the relaxation time upon the cessation of steady flow and $k$ is a parameter that is related to a critical stress value, below which the material exhibits primary creep. Later we will show that $\lambda$ is a structural relaxation time, i.e. a structural built up time, whereas $k$ can be interpreted as a kinetic constant for structure breaking down.

In the present work, the kinetic equation of the Fredrickson model (Eq. (1)) is used coupled to the upper-convected Maxwell constitutive equation to account for the Non-Newtonian and the thixotropic and antithixotropic behavior reported for viscoelastic micellar solutions and lamellar liquid crystalline dispersions under shear flow [6–10]. The Maxwell equation can be written as [21]

$$\tau + \delta(r, t)\overset{\nabla}{\tau} = \frac{2D}{\varphi(r, t)}, \tag{2}$$

where $\overset{\nabla}{\tau}$ is the codeformational derivative of the stress tensor, $\delta[=(G_0\varphi)^{-1}]$, is a structure-dependent relaxation time and $G_0$ is the instantaneous relaxation modulus.

## 2. Results

### 2.1. Steady simple shear flow

For simple shear flow, Eqs. (1) and (2) can be expressed as the following scalar equations:

$$\frac{\mathrm{d}\varphi}{\mathrm{d}t} = \frac{(\varphi_0 - \varphi)}{\lambda} + k(\varphi_\infty - \varphi)\tau_{12}\dot{\gamma}, \tag{3}$$

$$\tau_{12} + \frac{1}{G_0\varphi}\frac{\mathrm{d}\tau_{12}}{\mathrm{d}t} - \frac{\tau_{22}\dot{\gamma}}{G_0\varphi} = \frac{\dot{\gamma}}{\varphi}, \tag{4}$$

$$N_1 + \frac{1}{G_0\varphi}\frac{\mathrm{d}N_1}{\mathrm{d}t} = \frac{2\tau_{12}\dot{\gamma}}{G_0\varphi} \tag{5}$$

and

$$N_2 + \frac{1}{G_0\varphi}\frac{\mathrm{d}N_2}{\mathrm{d}t} = 0, \tag{6}$$

where $N_1(\equiv \tau_{11} - \tau_{22})$ and $N_2(\equiv \tau_{22} - \tau_{33})$ are the first and second normal stress differences, respectively. In what follows, the third term in the left hand side of Eq. (4) will be neglected due to $\tau_{22}$ being small. Also, for simplicity, the subscripts of $\tau_{12}$ will be dropped.

For simple steady shear flow, the time derivatives in Eqs. (3)–(6) become zero. The combination of Eqs. (3) and (4) with their time derivatives set equal to zero, yields a quadratic equation in $\varphi$, whose non negative root gives the steady state fluidity:

$$\varphi_{SS} = \tfrac{1}{2}[-(k\lambda\dot{\gamma}^2 - \varphi_0) + ((k\lambda\dot{\gamma}^2 - \varphi_0)^2 + 4k\lambda\dot{\gamma}^2\varphi_\infty)^{1/2}]. \tag{7}$$

Eq. (7) gives the shear rate dependence of the steady state fluidity, where its limits at zero and at very large shear rates are $\varphi_0$ and $\varphi_\infty$, respectively.

Fredrickson [20] showed that when $\varphi_0 = 0$, the material behaves as a Bingham plastic (i.e. an apparent yield stress is observed); when $\varphi_0 = \varphi_\infty$, the fluid is Newtonian; and when $0 < \varphi_0 < \varphi_\infty$, the fluid is pseudoplastic and shows a Newtonian plateau with viscosity equal to $\varphi_0^{-1}$ at low shear rates and other plateau at very high shear rates with viscosity equal to $\varphi_\infty^{-1}$.

Fig. 1 shows plots of the steady shear viscosity versus shear rate with identical values of $\varphi_0$, $k$ and $\lambda$ but different values of $\varphi_\infty$. Here, Newtonian behavior (when $\varphi_0 = \varphi_\infty$), shear-thinning behavior (whenever $\varphi_0 < \varphi_\infty$) or shear-thickening behavior (whenever $\varphi_0 > \varphi_\infty$) is observed—the latter case was not examined by Fredrickson [20].

The substitution of $\varphi_{ss}$ in Eq. (5) with $\mathrm{d}N_1/\mathrm{d}t = 0$ gives

$$N_1 = \frac{2\dot{\gamma}\tau}{G_0\varphi_{ss}}. \tag{8}$$

For small enough values of $\dot{\gamma}$, $\varphi_{ss}$ tends toward $\varphi_0$ and from Eq. (4), $N_1$ shows a quadratic dependence on $\dot{\gamma}$ in this limit; likewise, for very high shear rates, $\varphi_{ss}$ tends toward $\varphi_\infty$ and $N_1$ increases again in a quadratic fashion with $\dot{\gamma}$ (inset in Fig. 1).

Fig. 2 shows plots of shear stress versus shear rate for different values of $\varphi_0$. Notice that at low values of $\varphi_0$ there is an apparent yield stress. However, amplification of the scale shows that the stress goes to zero as the applied shear rate goes to zero, except when $\varphi_0 = 0$ (inset in Fig. 2); in this case, Bingham plastic-like behavior is observed, i.e. a yield stress is detected. Fredrickson [20] argued that when $\varphi_0 = 0$, an infinite stress is required to start building up the fluidity of the material, which is not physically possible; so, he concluded that there is not a true yield stress. However, from Eq. (3) with $\varphi_0 = 0$ one can show that

$$\varphi = \varphi_\infty[1 - (\tau_c/\tau)^2], \tag{9}$$

where $\tau_c[\equiv (k\lambda\varphi_\infty)^{-1/2}]$ is the plateau value of the stress (inset in Fig. 2) and is as good a yield stress as the Bingham one.

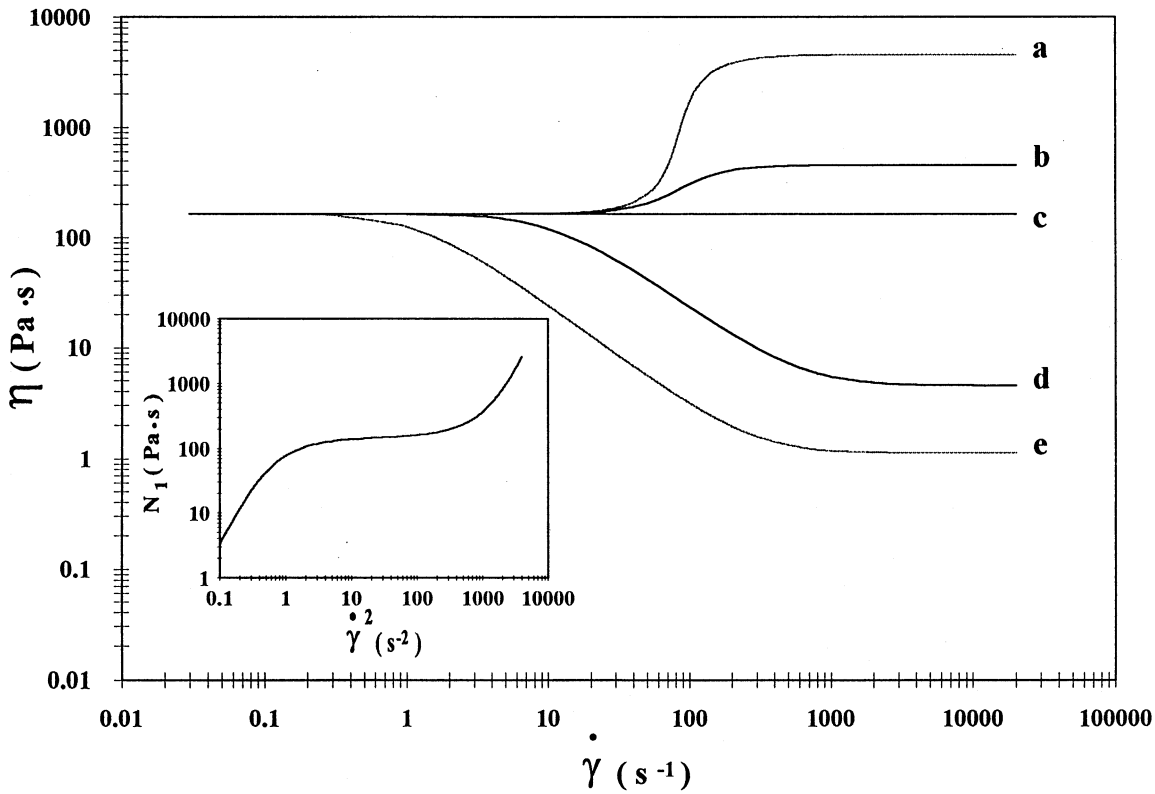


Fig. 1. Shear viscosity vs. shear rate as a function of $\varphi_\infty$ in (Pa s)$^{-1}$: (a) 0.0002; (b) 0.002; (c) 0.0053; (d) 0.20; (e) 1. Inset: First normal stress difference as a function of $\dot{\gamma}^2$ for curve e. The parameters used were $\varphi_0 = 0.0053$ (Pa s)$^{-1}$; $G_0 = 185$ Pa; $k = 3.9 \times 10^{-5}$ Pa$^{-1}$; $\lambda = 0.14$ s.

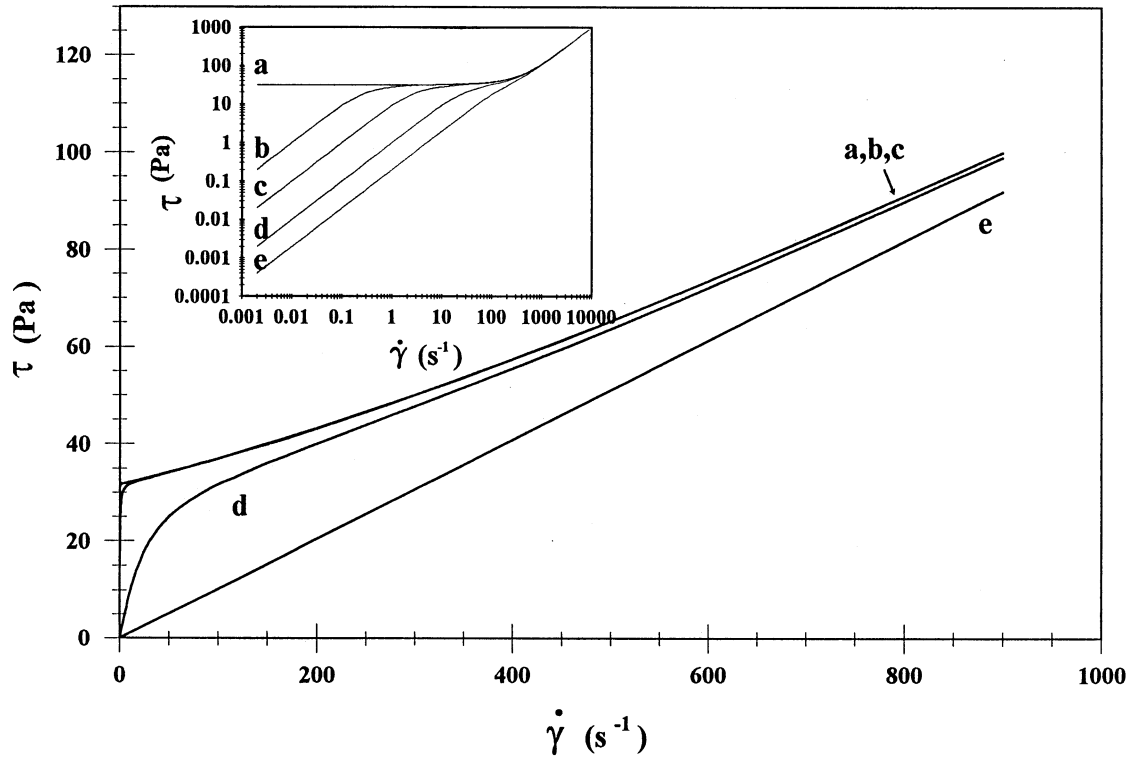


Fig. 2. Shear stress vs. shear rate as a function of $\varphi_0$ in (Pa s)$^{-1}$: (a) 0.0; (b) 0.0001; (c) 0.001; (d) 1.0; (e) 10.5. Inset: Enlargement of scale in log–log mode. The parameters used were $\varphi_\infty = 10.5$ (Pa s)$^{-1}$; $G_0 = 185$ Pa; $k = 3.9 \times 10^{-5}$ Pa$^{-1}$; $\lambda = 0.14$ s.

### 2.2. Stress relaxation after cessation of steady shear flow

In this type of experiment, a sample is sheared at constant and steady shear rate ($\dot{\gamma}_{ss}$). At time $t = 0$, the flow is suddenly stopped and the relaxation of the stress is followed as a function of time. Hence, one sets $\dot{\gamma} = 0$ in Eq. (3). The integration of the resulting equation, with the initial condition $\varphi(0) = \varphi_{ss}$, yields

$$\varphi = \varphi_0 + (\varphi_{ss} - \varphi_0)e^{-t/\lambda}. \tag{10}$$

The substitution of Eq. (10) in Eq. (4) with $\dot{\gamma} = 0$ and the integration with the initial condition $\tau(0) = \tau_{ss}$, produces

$$\tau = \tau_{ss} \exp[-G_0(\varphi_0 t + \lambda(\varphi_{ss} - \varphi_0)(1 - e^{-t/\lambda}))]. \tag{11}$$

For very low values of steady shear rate, where $\varphi_{ss}$ tends to $\varphi_0$, the stress should relax monoexponentially with a time constant given by $(G_0\varphi_0)^{-1}$, which is equal to the Maxwell relaxation time.

Eq. (11) has two limits: one at short times and another one at long times. At short times, a series expansion of $e^{-t/\lambda}$ in Eq. (11) gives, after neglecting terms of order three and higher, that

$$\tau = \tau_{ss} \exp\left[ - G_0\left( \varphi_{ss} t + \frac{(\varphi_{ss} - \varphi_0)t^2}{2\lambda} + \ldots \right)\right]. \tag{12}$$

When the quadratic term is neglected, a single time constant given by $(G_0\varphi_{ss})^{-1}$ is recovered. A plot of $\log(\tau/\tau_{ss})$ versus time (Fig. 3) follows straight lines at very short times, with larger negative slopes than $(G_0\varphi_0)^{-1}$ due to $\varphi_{ss}$ being larger than $\varphi_0$ for shear thinning fluids. Notice that the slope of $\log(\tau/\tau_{ss})$ versus time depends on the steady state conditions prior to the relaxation process due to $\varphi_{ss}$ increasing with shear rate; hence the relaxation becomes faster as the value of $\varphi_{ss}$ increases (Fig. 3). The limiting value of $\varphi_{ss}$ is $\varphi_\infty$, which is reached at very high shear rates. In this case, the shortest relaxation constant is equal to $\eta_\infty G_0^{-1}$ and the initial slope reaches its steepest possible value.

The time range of validity of the linear approximation can be estimated by equating the linear and quadratic terms of the argument in Eq. (12). This shows that the linear approximation is valid for times smaller than $4\varphi_{ss}\lambda/(\varphi_{ss} - \varphi_0)$. This limit has been verified experimentally [6].

For long times, Eq. (11) can be written as

$$\tau = A\tau_{ss} \exp[ - G_0\varphi_0 t], \tag{13}$$

where $A = \exp[ - G_0\lambda(\varphi_{ss} - \varphi_0)]$. In this situation, the relaxation time corresponds again to the Maxwell relaxation time. However, the extrapolation at time zero of the stress curves gives stress values smaller than $\tau_{ss}$ by a factor equal to $\exp[ - G_0\lambda(\varphi_{ss} - \varphi_0)]$, which depends on the steady state flow conditions prior to cessation of flow (Fig. 3).

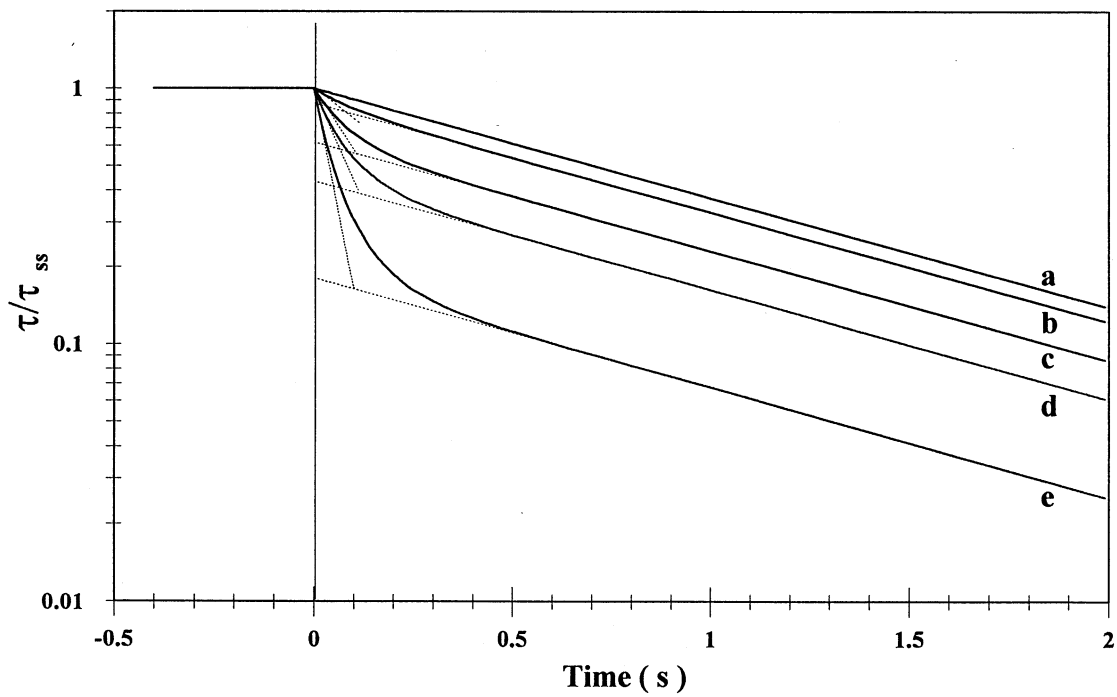


Fig. 3. Normalized shear stress after cessation of steady flow ($\tau/\tau_{ss}$) vs. time as a function of shear rate ($s^{-1}$): (a) 0.1; (b) 1; (c) 3; (d) 5; (e) 10. The parameters used: $\varphi_0 = 0.0053$ (Pa s)$^{-1}$; $\varphi_\infty = 10.5$ (Pa s)$^{-1}$; $k = 3.9 \times 10^{-5}$ Pa$^{-1}$; $\lambda = 0.14$ s; $G_0 = 185$ Pa. $\tau_{ss}$ is the steady stress prior to the cessation of flow.

It is noteworthy that the relaxation process at short times is governed by a time constant that depends on the steady state fluidity ($\varphi_{ss}$) prior to the relaxation. On the other hand, the relaxation at long times is governed by a time constant that corresponds to the Maxwell relaxation time. Therefore, at long times one should expect lines with identical slopes whose ordinates are functions of the magnitude of ($\varphi_{ss} - \varphi_0$) (Fig. 3). Consequently, Eq. (13) tends toward $\exp(-G_0\varphi_0 t)$ as $\varphi_{ss} \to \varphi_0$. Eq. (13) and its limit have been verified experimentally [6].

### 2.3. Step change in stress and creep

In this case, the shear stress on the fluid is suddenly changed from $\tau_0$ to $\tau_1$, and it remains at the latter value for subsequent times. Therefore, Eq. (3) can be written as

$$\frac{d\varphi}{dt} = \frac{(\varphi_0 - \varphi)}{\lambda} + k(\varphi_\infty - \varphi)\tau_1^2\varphi. \tag{14}$$

This equation, in turn, can be written in the form of the Ricatti equation, i.e.

$$\frac{d\varphi}{dt} = -k\tau_1^2\varphi^2 + \left(k\tau_1^2\varphi_\infty - \frac{1}{\lambda}\right)\varphi + \frac{\varphi_0}{\lambda}. \tag{15}$$

Performing the change of variable $\varphi = \varphi_{ss} + y^{-1}$ in Eq. (15) with the initial condition, $\varphi(0) = \varphi_{00}$ (where $\varphi_{00}$ is the fluidity corresponding to the stress $\tau_0$, which can be any steady/unsteady initial stress), and with $\varphi(\infty) = \varphi_{ss}$, it yields, after some manipulations, that [22]:

$$\varphi(t) = \varphi_{ss} + \left[\left(\frac{k\tau_1^2}{\theta} + \frac{1}{\varphi_{00} - \varphi_{ss}}\right)e^{\theta t} - \frac{k\tau_1^2}{\theta}\right]^{-1}, \tag{16}$$

where $\theta = k\tau_1^2(2\varphi_{ss} - \varphi_\infty) + \lambda^{-1}$.

Fig. 4 shows the variation of viscosity as a function of time, calculated with Eq. (16), due to successive step changes in shear stress at constant time intervals. In this case, the step is applied after the sample has reached its steady shear rate value. Notice how the change in viscosity becomes steeper as the stress increases because, presumably, disruption of structure of the sample upon increasing shear stress.

The model also allows the calculation of the compliance, $J(\tau, t)$ ($= \gamma/\tau_1$), according to

$$J(\tau, t) = \int_0^t \varphi(t)\, dt. \tag{17}$$

Hence, after integration, the substitution of Eq. (16) into Eq. (17) yields

$$J(\tau_1, t) = \left(\varphi_0 - \frac{\theta}{k\tau_1^2}\right)t + \frac{1}{k\tau_1^2}\ln\left[\frac{\varphi_\infty k\tau_1^2}{\theta}(1 - e^{\theta t}) + e^{\theta t}\right]. \tag{18a}$$

Fig. 5 shows the compliance and the viscosity versus time for several applied stresses. For stresses smaller than $\tau_c[\equiv (k\lambda\varphi_\infty)^{-1/2}]$, there is a primary creep region at short times, corresponding to an initial elastic response of variable shear rate. At long times, the sample flows with constant shear rate and $J(t)$ follows a straight line with slope $\varphi_0$. The viscosity, on the other hand, increases from $\eta_\infty(\equiv \varphi_\infty^{-1})$ at short times (corresponding to its value at high frequencies or high shear rates) up to $\eta_0$ at a long times. Notice that the primary creep region

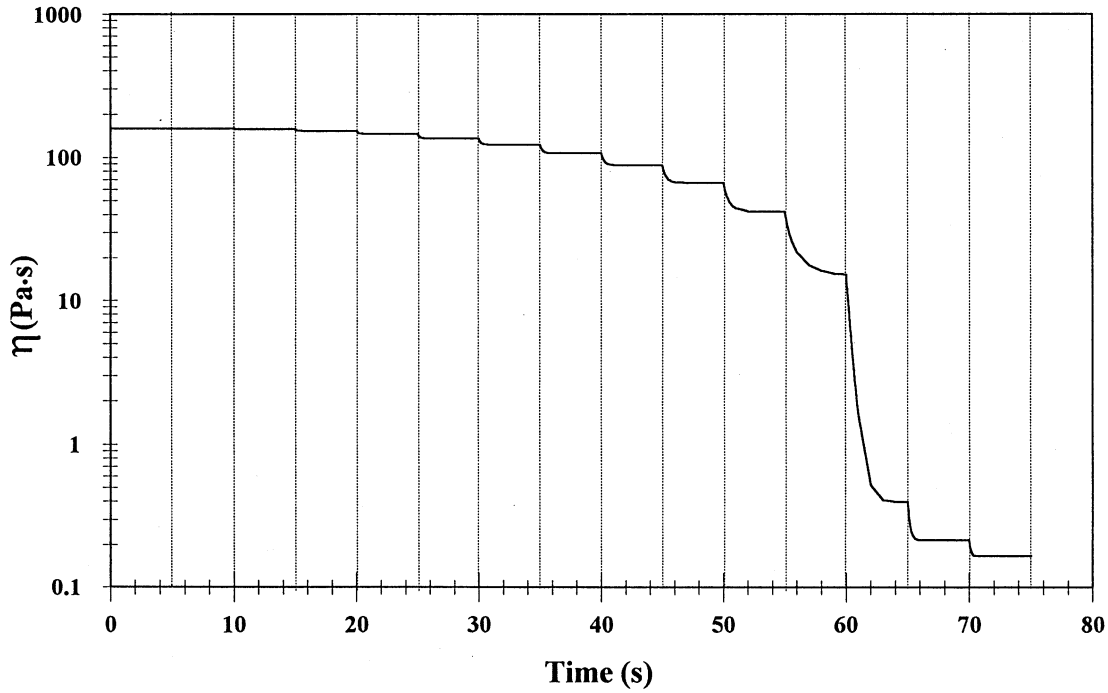


Fig. 4. Viscosity as a function of time after successive step changes in stress ($\Delta\tau = 10$ Pa). The parameters used are the same as in Fig. 3.

appears simultaneously to the region where the viscosity is almost constant with value $\eta_\infty$. For stresses slightly larger than $\tau_c$, the compliance attains a slope equal to $\varphi_{ss}(>\varphi_0)$ at long times (curve *d* in Fig. 5). For stresses much larger than $\tau_c$, the limiting slope at short and long times in the compliance curve tends to $\varphi_\infty$, i.e. there is a negligible primary creep. The viscosity in this case is constant and equal to $\eta_\infty$.

The time required to reach steady state can be found from Eq. (16) in the limit $t \to \infty$. It turns out that for times equal to $\theta^{-1}$ the slope of $J(\tau_1, t)$, has reached 80% of its steady state value, $\varphi_0$, whereas for times longer than $4\theta^{-1}$, this value is 98.8% of $\varphi_0$.

Fig. 6 depicts the behavior of $\theta\lambda$ as a function of the applied reduced stress ($\tau/\tau_c$) The region where $\tau < \tau_c(=1/\sqrt{k\lambda\varphi_\infty})$ is the creep region corresponding to the limiting slope, $\varphi_0$, at long times, where $\theta\lambda$ varies from 1 down to zero. When $\tau > \tau_c$, $\theta\lambda$ increases with increasing reduced stress and corresponds to the flow region where the limiting slope at long times is $\varphi_{ss}$. The largest slope corresponds to $\varphi_{ss} = \varphi_\infty$, which is attained at very large stresses; in this case, $\theta\lambda = 1 + (\tau/\tau_c)^2$.

It is useful to recast Eq. (18a) in terms of $\theta\lambda$ and $\tau/\tau_c$ to illustrate the two regimes of behavior expected from the shape of $\theta\lambda$ in Fig. 6:

$$J(\tau_1, t) = \left(\varphi_0\lambda - \frac{\theta\lambda^2\varphi_\infty}{(\tau_1/\tau_c)^2}\right)t_r + \frac{\varphi_\infty\lambda}{(\tau_1/\tau_c)^2}\ln\left[\frac{(\tau_1/\tau_c)^2}{\theta\lambda}(1 - e^{\theta\lambda t_r}) + e^{\theta\lambda t_r}\right], \tag{18b}$$

where $t_r$ is the reduced time $t/\lambda$. When $\tau/\tau_c \to 0$ and for significant lengths of time, Eq. (18b) renders $J(t) = \varphi_\infty \lambda + \varphi_0 t$ which represents a straight line with intercept $\varphi_\infty \lambda$, the steady state compliance, $J_e^0$ [24]. One may thus view the creep compliance as composed of 'an elastic part' $J_e^0 = \varphi_\infty \lambda$ and a 'viscous part' $\varphi_0 t$. Notice that $J_e^0 = 1.47$ for curve a in Fig. 5. On the other hand, when $\tau/\tau_c \gg 1$, $J(t) = \varphi_\infty t$. It is interesting to point out that at short times, Eq. (18b) gives, $J(t) \approx \varphi_\infty t$ for all magnitudes of the stress. This is the initial slope of curves a–d in Fig. 5.

### 2.4. Step change in shear rate

Here, a sample is being sheared at a steady shear rate ($\dot{\gamma}_{ss}$); suddenly at time $t = 0$, the shear rate is changed in step fashion to $\dot{\gamma}_1$. For this situation, Eqs. (3) and (4) apply with $\dot{\gamma} = \dot{\gamma}_1$ and with the initial conditions, $\varphi(0) = \varphi_{ss}$ and $\tau(0) = \tau_{ss}$. Eqs. (3)–(5) have to be solved numerically. However, it is possible to find analytical solutions for the inception of flow, i.e. when $t < 0$, $\dot{\gamma} = 0$ and $t \geq 0$, $\dot{\gamma} = \dot{\gamma}_1$. In this case, Eq. (4) gives

$$\tau[\varphi(t)] = \frac{\dot{\gamma}_1}{\varphi}\,(1 - e^{-G_0 \varphi t}). \tag{19}$$

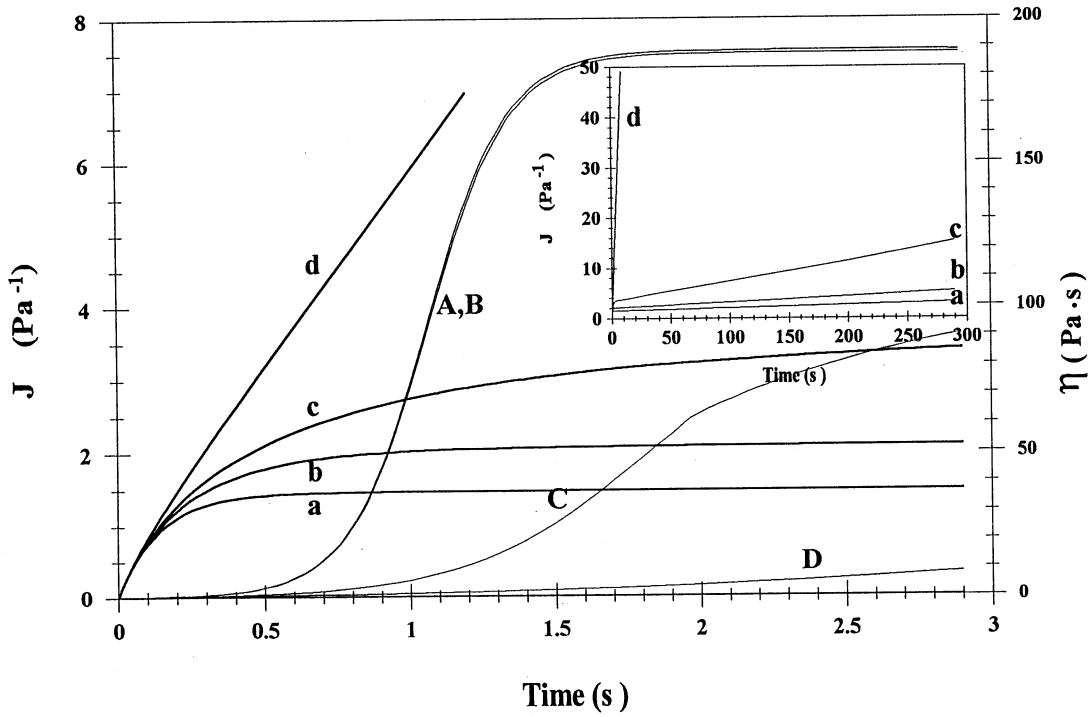


Fig. 5. Compliance (small caps) and viscosity (capital caps) vs. time as a function of the applied stress (Pa): (a, A) 1; (b, B) 100; (c, C) 130; (d, D) 200. Inset: enlargement of scale for the compliance. The parameters used are the same as in Fig. 3.

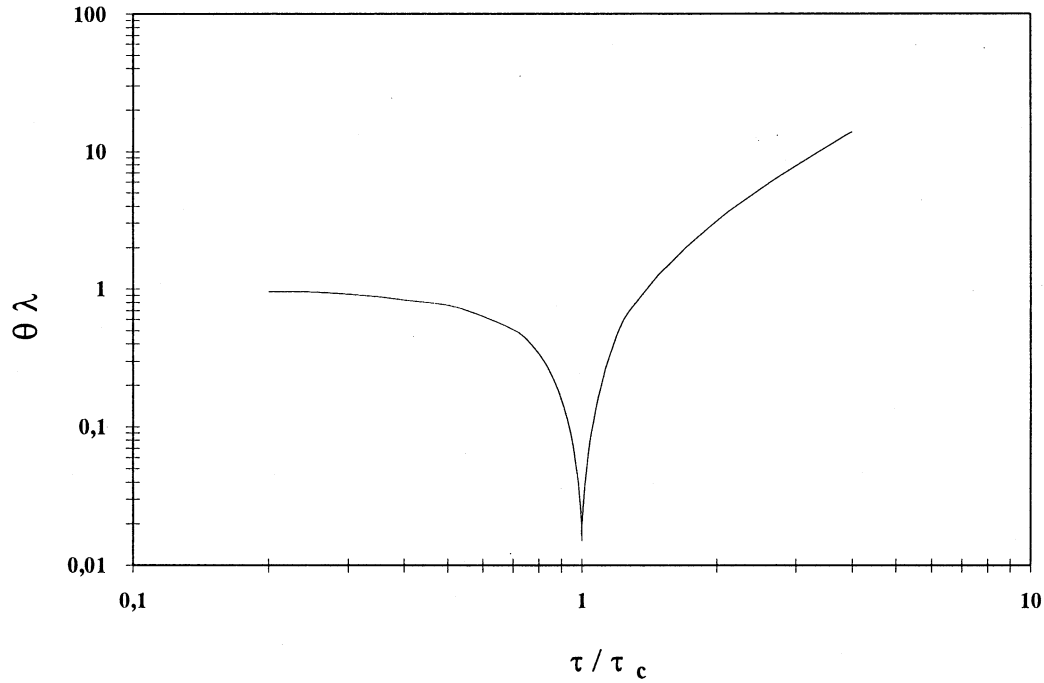


Fig. 6. $\theta\lambda$ as a function of the normalized applied stress ($\tau/\tau_c$). $\theta$ is defined in text and $\tau_c$ is the plateau stress.

It is clear that a very low shear rates, $\varphi \approx \varphi_0$ and $d\varphi/dt \approx 0$ in Eq. (3). In this situation, Maxwellian behavior is followed with a time constant equal to $(G_0\varphi_0)^{-1}$ and furthermore $\eta^+ \to \eta_0$ in the limit of long times.

For higher shear rates, as in the case of step change in the stress, the fluidity at very short times is $\varphi_\infty$ (corresponding to its value at high frequencies or high shear rates) and Eq. (3) becomes

$$\varphi(t) = \varphi_0 + (\varphi_\infty - \varphi_0)\, e^{-t/\lambda}. \tag{20}$$

In this case, stress is given by a combination of Eqs. (19) and (20).

At long times, in the intermediate shear rate region, $\varphi \gg \varphi_0$ and $\varphi_\infty \gg \varphi$, resulting in Eq. (3) becoming, (with $\tau \cong \dot{\gamma}/\varphi$ from Eq. (19))

$$\frac{d\varphi}{dt} = -\frac{\varphi}{\lambda} + \frac{k\varphi_\infty \dot{\gamma}^2}{\varphi}, \tag{21}$$

which, after integration, renders

$$\varphi(t) = [\varphi_\infty^2\, e^{-2t/\lambda} + k\lambda\varphi_\infty \dot{\gamma}^2(1 - e^{-2t/\lambda})]^{1/2}. \tag{22}$$

Note that as $t \to \infty$, $\varphi(t) \to \dot{\gamma}_1/\tau_c = \varphi_{ss}$ and the stress tends to its steady state value, $\tau_c$ (the plateau stress).

Fig. 7 shows the stress growth coefficient, $\eta^+(t)$, calculated numerically for the inception of shear flow, as a function of shear rate. For low shear rates, $\eta^+(t)$ follows a Maxwellian behavior

with a time constant equal to $(G_0\varphi_0)^{-1}$ (curve *a* in Fig. 7). As $\dot{\gamma}$ increases, $\eta^+$ exhibits overshoots which become bigger as the applied shear rate increases (curves b, c, y, d in Fig. 7). Of course, the model predicts that $\eta^+(t) \to \eta_{ss}$ as $t \to \infty$.

The analytical approximations for short and long times in the intermediate shear rate region ($\dot{\gamma} = 40\ s^{-1}$ for this case), given by Eqs. (20) and (22), are compared with the numerical solution in the inset of Fig. 7. Both approximations follow closely the numerical solution at short and long times, although both depart from the exact solution outside their respective time range of application. Notice that at the inception of flow, $\varphi(t \to 0) = \varphi_\infty$, the fluidity attains its maximum value which corresponds to the initial magnitude of $\eta^+(t)$ at very short times. The variation of $\varphi$ with time is independent of the destruction term in Eq. (3). This is a purely elastic response whose contribution decreases as time evolves; in turn, the destruction of structure manifests at times longer than the overshoot time scale. Thus, curve I in Fig. 7 signals the limit of elastic response.

### 2.5. Instantaneous stress relaxation

Here, a sample initially at rest, is suddenly subjected to a given deformation, $\gamma_1$, and immediately the flow is stopped and the stress is allowed to relax. In this case, Eqs. (3)–(5) have to be solved numerically. An analytical solution can be obtained, however, by allowing the sample initially at rest, to be deformed for a very short period of time ($t_1$); then the flow is

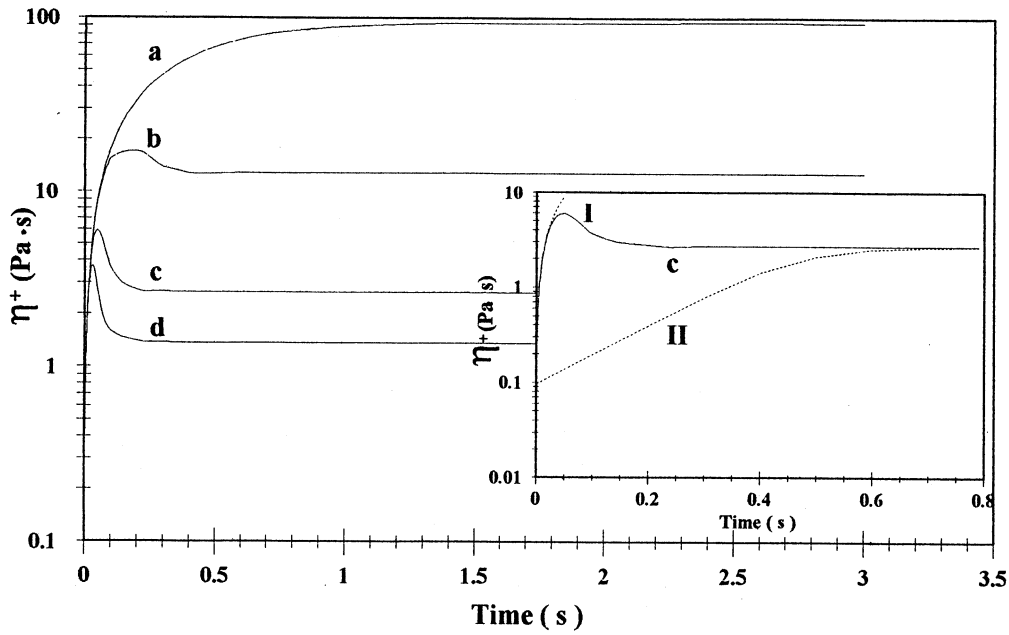


Fig. 7. Stress growth coefficient vs. time upon interception of flow for different values of applied shear rate ($s^{-1}$): (a) 1; (b) 10; (c) 40; (d) 50. The parameters used are the same as in Fig. 3. Inset: Comparison of numerically obtained curve c with approximations for short time (curve I) and long time (curve II) given by Eq. (20) and Eq. (22), respectively.

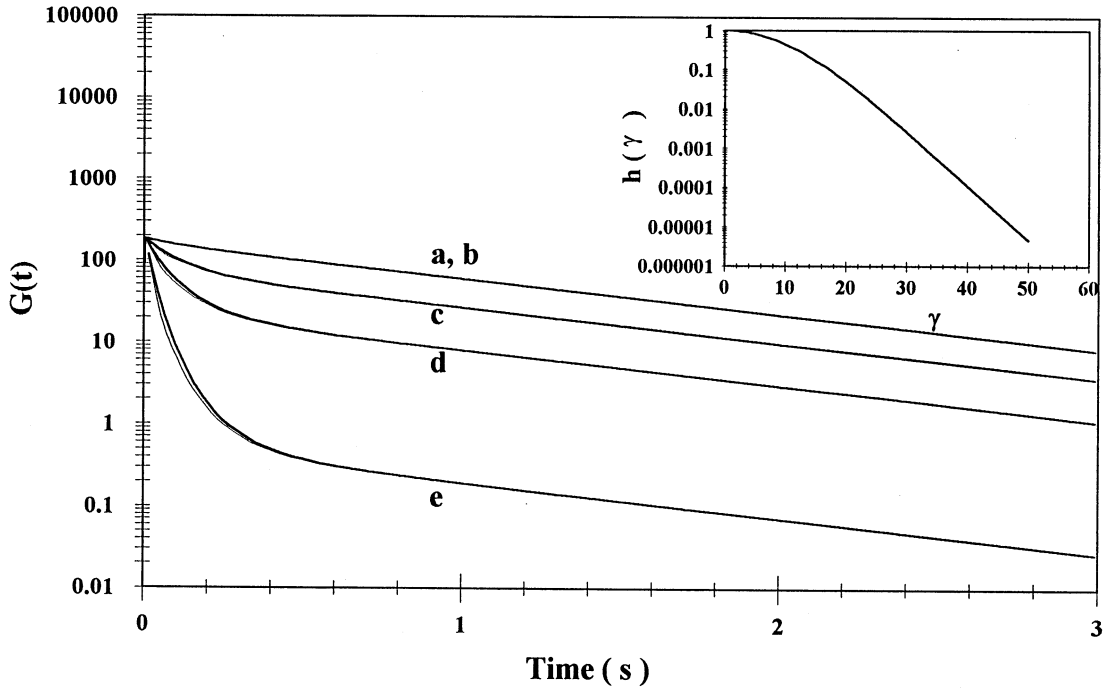


Fig. 8. Relaxation modulus as a function of time for different values of applied shear strain (%): (a) 0.1; (b) 0.5; (c) 1.0; (d) 2.0; (e) 3.0. Thick line: numerical solution; thin line: solution given by Eq. (23) divided by $\gamma$. The parameters used are the same as in Fig. 3. Inset: Damping function as a function of strain.

stopped and the stress is allowed to relax. This situation is more realistic that an instantaneous deformation. In fact, in the rheometer employed here, the applied deformation lasts $\sim 0.05$ s. In this case, the deformation history can be represented by

$$\dot{\gamma}\begin{cases} 0 & t<0, \\ \dot{\gamma}_1 \quad \text{for} & 0\le t\le t_1, \\ 0 & t>t_1, \end{cases}$$

Eqs. (3)–(5) describe this process with $\dot{\gamma}=\dot{\gamma}_1$. After a period $t_1$, the flow is stopped and the stress relaxation is given by Eq. (11) with $\tau(t_1)$ instead of $\tau_{ss}$ and with $\varphi_{ss}=\varphi(t_1)$, since these material functions have not yet reached their steady state values. Hence

$$\tau=\tau(t_1)\exp[-G_0(\varphi_0 t+\lambda(\varphi(t_1)-\varphi_0)(1-\mathrm{e}^{-t/\lambda}))], \tag{23}$$

where $\varphi(t_1)$ is given by Eq. (20) which gives the fluidity at short times after a step change in shear rate.

Fig. 8 depicts a semi-logarithmic plot of the relaxation modulus, $G(t)=\tau(t)/\gamma$ versus time as a function of shear strain. For low values of applied strain, a linear viscoelastic behavior is

predicted, i.e. $G(t)$ is independent of $\gamma$ (lines a and b in Fig. 8). For larger values of strain, however, $G(t)$ depends on $\gamma$ (lines c to e in Fig. 8). This behavior corresponds to the nonlinear viscoelastic regime. The solution given by Eq. (23) closely follows the numerical solution as long as $t_1$ is sufficiently small [13]. In fact, the stress given by Eq. (23) with $t_1 = 0.05$ s agrees with the stress calculated numerically within 0.9%.

At long times, Eq. (23) reduces to an expression equal to Eq. (13) with $\tau_{ss} = \tau(t_1)$. The intercept of the plot of $\log(\tau/\tau_{ss})$ versus time is $-G_0\lambda(\varphi(t_1) - \varphi_0)$. For this situation, Eq. (23) divided by $\gamma[\equiv \dot{\gamma}t_1]$ may be expressed as

$$G(t) = G_l(t)h(\gamma). \tag{24}$$

Here $G_l(t)$ is the linear relaxation modulus and $h$ is the damping function, which is usually defined as $[\exp(-K\gamma)]$, where $K$ is the damping coefficient [25]. Inspection of Eq. (13) with $\tau_{ss} = \tau(t_1)$ and $\varphi_{ss} = \varphi(t_1)$ shows that $G_l(t) = (\tau(t_1)/\dot{\gamma}t_1)\exp(-G_0\varphi_0 t)$ and $h = \exp[-G_0\lambda(\varphi(t_1) - \varphi_0)]$, which provides a theoretical ground to the empirical treatment proposed elsewhere [25].

Eq. (24) indicates that the stress relaxation modulus can be separated in a time-dependent part (the relaxation function) and a strain-dependent part (the damping function). The non-linear behavior of the fluid can be quantified by measuring the magnitude of the ordinate at $t = 0$ of the curve of log $G(t)$ versus time. The inset in Fig. 8 shows $h$ as a function of deformation. The damping coefficient, $K$, which is the slope of this curve, has a value near 0 at low deformations (ca. 2%),within the linear viscoelastic region. $K$ reaches a constant value equal to 0.14 at higher deformations, i.e. the damping function decays monoexponentially with deformation. In between these regimes, $K$ varies with deformation. Laun [26] reported a similar behavior of $h$ as a function of deformation for polymer melts.

### 2.6. Transient stress cycles

Attention is given here to the predictions of the model in time-dependent complex flow histories produced by a controlled stress rheometer in an exponential stress mode. Exponential shear flow is a strong flow since the distance between material elements of the fluid increases exponentially with time. Nevertheless, this type of flow is not devoid of vorticity and hence it does not possess the strength of a pure extensional deformation. In this regard, exponential shear flow is kinematically characterized by shear and extensional components.

The exponentially increasing–decreasing shear stress histories yield thixotropic loops in micellar solutions of CTAT and in other microstructured surfactant-based fluids [6,7]. In these experiments, the stress is increased exponentially at time $t = 0$ from a preset value ($\tau_0$) to a prescribed maximum stress ($\tau_f$) at $t = t_1$. Subsequently, $\tau_f$ can be kept constant for a given period of time. In the final stage at $t = t_2$, stress is decreased exponentially with time to $\tau_0$ at the same rate as in the increasing mode. Also, two or more consecutive cycles can be performed in the sample with or without a rest period between the cycles. There are three main variables in this type of experiments: the magnitude of the final stress, $\tau_f$, the rate of change of stress, $a$, and the duration of the interval of constant stress, $(t_2 - t_1)$.

The shear history in this case is given by the following expressions:

$$\tau = \begin{cases} \tau_0 \, e^{at} & 0 \le t \le t_1, \\ \tau_f \quad \text{for} & t_1 \le t \le t_2, \\ \tau_0 \, e^{-at} & t_2 \le t \le t_3. \end{cases} \tag{25}$$

The substitution of these equations in Eq. (3) and Fig. 4 yields

$$\tau + \frac{1}{G_0 \varphi} \langle \pm \rangle a\tau = \frac{\dot{\gamma}}{\varphi}, \tag{26}$$

$$\frac{d\varphi}{dt} = \frac{(\varphi_0 - \varphi)}{\lambda} + k(\varphi_\infty - \varphi)\dot{\gamma}\tau. \tag{27}$$

The combination of Eqs. (26) and (27) gives

$$\frac{d\varphi}{dt} = \frac{(\varphi_0 - \varphi)}{\lambda} + k(\varphi_\infty - \varphi)\tau^2 \left( \varphi \langle \pm \rangle \frac{a}{G_0} \right). \tag{28}$$

This equation has no analytical solution; therefore, it was solved numerically for the different situations presented in the following.

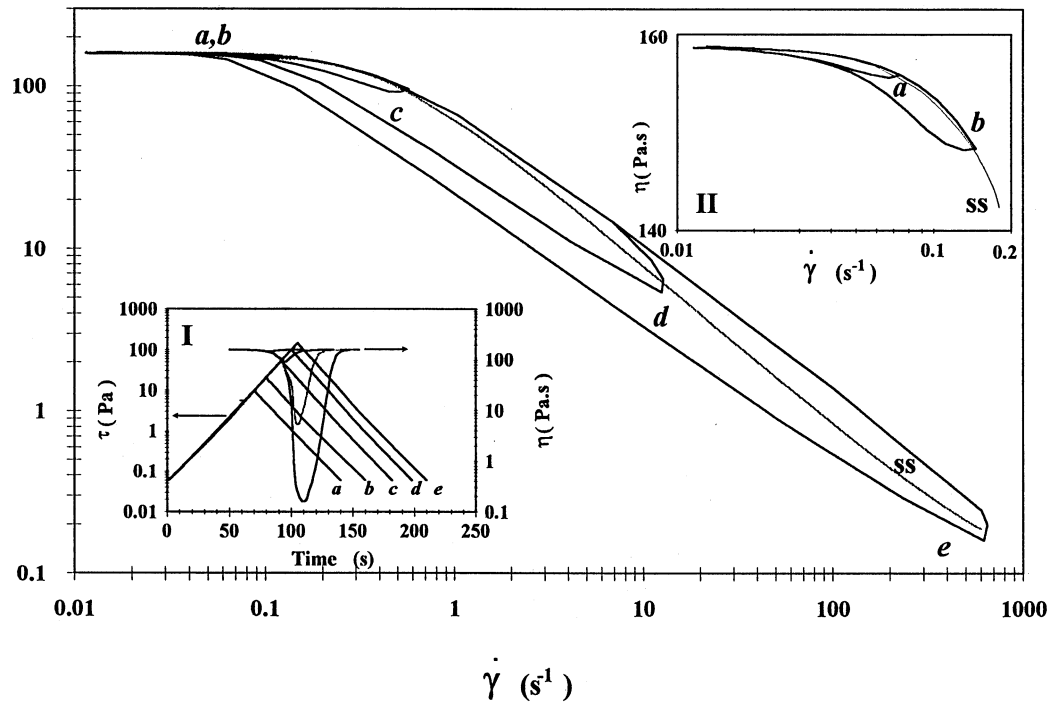


Fig. 9. Shear viscosity as a function of shear rate for exponentially increasing and decreasing stress cycles. Initial stress is the same in all cycles ($\tau_0 = 0.1$ Pa) and final stress, $\tau_f$ is varied: (a) 10; (b) 20; (c) 50; (d) 100; (e) 150. The parameters used are the same as in Fig. 3. Inset I: Stress program applied and time response of viscosity. Inset II: Enlargement of the scale for curves a and b.

The effect of increasing the final stress, $\tau_f$, on the extent of thixotropy is shown in Fig. 9. The steady shear curve is included in this figure for comparison (curve ss in Fig. 9). The inset I in this figure depicts the applied stress program and the viscosity response as a function of time. All the relevant parameters of the model (i.e. $G_0$, $\delta$, $\lambda$, $\varphi_0$, $\varphi_\infty$ and $k$) were fixed in the simulations. When $\tau_f$ is small, i.e. levels of stress within the Newtonian region in steady shear, the thixotropic loops are very small, almost negligible (curves a and b in Fig. 9 and inset II). As $\tau_f$ increases, the extent of the thixotropic loops augments (curves c to e in Fig. 9). Also, as expected, the shear viscosity at the maximum applied stress becomes smaller as the value of $\tau_f$ increases. Hence, in the increasing shear mode, structure breaks down by the application of increasing stress. Therefore, as the applied stress becomes larger, more structure is broken down, and consequently, lower viscosities are obtained. Notice that the time when $\tau_f$ is reached does not coincide with that when the minimum in viscosity is observed (inset I in Fig. 9). This implies that the breaking down of structure continues for a time even after the stress has become smaller than $\tau_f$, i.e. in the stress decreasing mode. Also, in the stress decreasing mode, structure begins to build up, first slowly and then faster as the applied stress becomes smaller. The rate of structure built up depends strongly on the structure relaxation time, $\lambda$, as it will be discussed later. This thixotropic behavior has been observed in elongated micellar solutions and liquid crystalline dispersions [6,7].

The effect of the rate of increase of shear stress, $a(\equiv \mathrm{d}\ln\tau/\mathrm{d}t)$, on the extent of the hysteresis loops is shown in Fig. 10. The applied stress program and the time response of the viscosity are

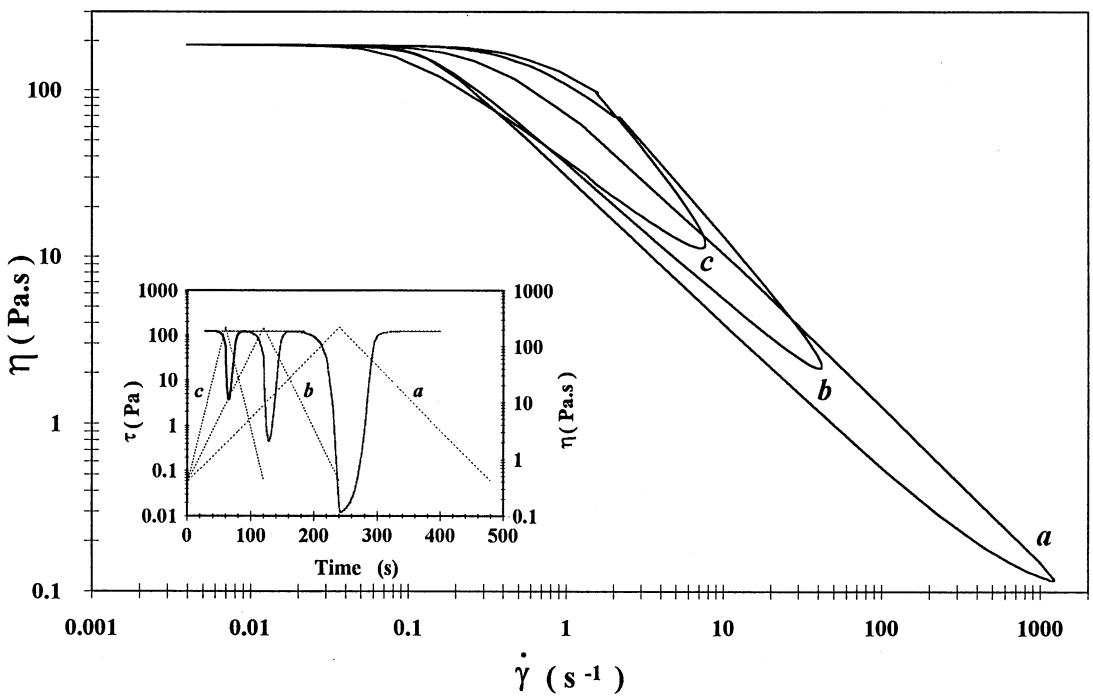


Fig. 10. Shear viscosity as a function of shear rate for exponentially increasing and decreasing stress cycles. Initial stress ($\tau_0 = 0.1$ Pa) and final stress ($\tau_f = 150$) are the same in all cycles, however, the ramp time, $a(= \mathrm{d}\ln\tau/\mathrm{d}t)$, is varied: (a) 0.014; (b) 0.028; (c) 0.033. The parameters used are the same as in Fig. 3. Inset: Stress program applied and time response of viscosity.

presented in the inset of this figure. The initial ($\tau_0$) and final ($\tau_f$) stresses are the same in all simulations. As is evident in Fig. 10, the size of the thixotropic loops increases as the time of the ramp used to reach the maximum level of the applied stress increases (i.e. with decreasing values of $a$).

The effect of the duration of the interval where $\tau_f$ is maintained is presented in Fig. 11. The applied stress program and the time response of the viscosity are depicted in the inset of this figure. The loops shown in this figure becomes larger as the duration of the interval of constant $\tau_f$ increases. Moreover, the value of $\eta$ at the end of the constant $\tau_f$ period diminishes as this period becomes longer. The explanation to this behavior is akin to the one given in the previous paragraph, i.e. the extent of disruption or breakdown of structure increases with both, the level of applied stress and the duration of the application of the stress.

The structural relaxation time, $\lambda$, has a strong influence on the size and the shape of the thixotropic loops. Fig. 12 depicts thixotropic loops obtained by the application of identical stress programs (inset) on samples with different values of $\lambda$ and identical values of the other parameters (i.e. $G_0$, $\delta$, $\varphi_0$, $\varphi_\infty$ and $k$). As discussed earlier, small values of $\lambda$ indicate a fast reformation of structure, i.e. a very labile structure, whereas large values of $\lambda$ imply a slower structure build up associated with a longer persistence lifetime. Two effects can be observed in Fig. 12 as the value of $\lambda$ is increased. One is that the extent of the thixotropic loops augments upon increasing the value of $\lambda$. In fact, the sample with the smaller value of $\lambda$ (fast reforming

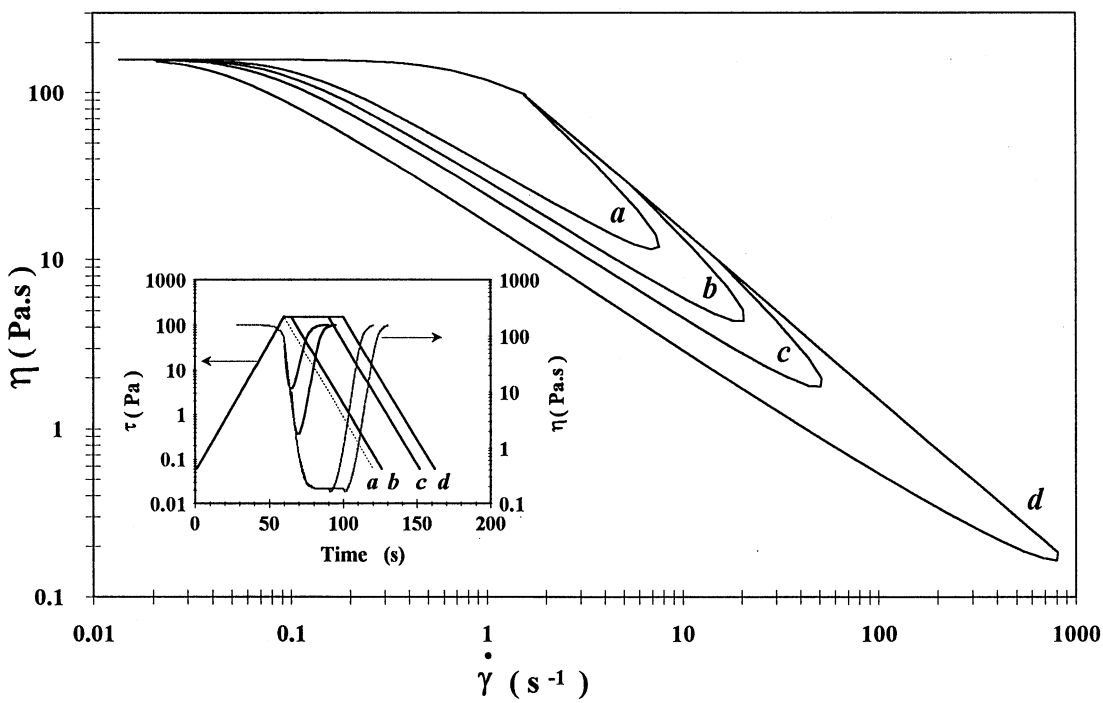


Fig. 11. Shear viscosity as a function of shear rate for exponentially increasing and decreasing stress cycles. Initial stress ($\tau_0 = 0.1$ Pa), final stress ($\tau_f = 150$) and $a(= \mathrm{d\ In}\ \tau/\mathrm{d}t) = 0.028$ are the same in all cycles, however, the period of time ($t_2 - t_1$) where $\tau_f$ is maintained and varied: (a) 0 s; (b) 10 s; (c) 30 s; (d) 40 s. The parameters used are the same as in Fig. 3. Inset: Stress program applied and time response of viscosity.

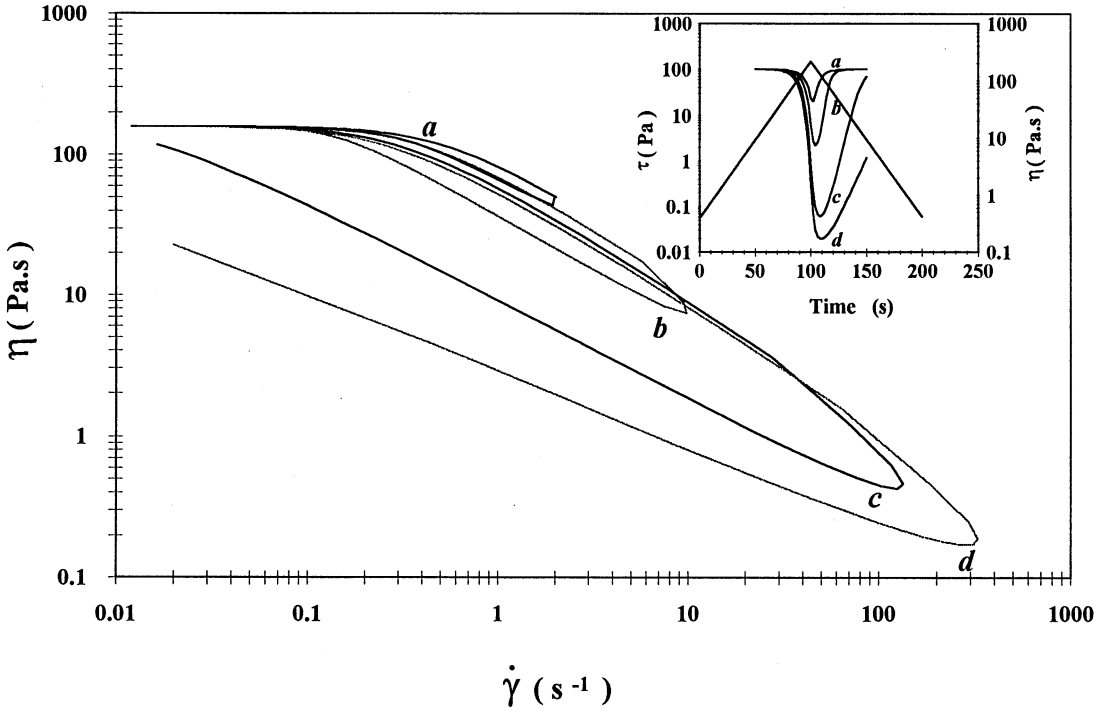


Fig. 12. Shear viscosity as a function of shear rate for exponentially increasing and decreasing stress cycles. Initial stress ($\tau_0 = 0.1$ Pa), final stress ($\tau_f = 100$) and $a(= \mathrm{d} \ln \tau/\mathrm{d}t) = 0.028$) are the same in all cycles. The parameters used are the same as in Fig. 3, with the exception of $\lambda$, which was varied: (a) 1 s; (b) 2 s; (c) 5 s; (d) 10 s. Inset: Stress program applied and time response of viscosity.

structure) exhibits the smallest thixotropic loop. The other effect is that as $\lambda$ increases, the loops tend to open up and the viscosity does not return to its initial value, $\eta_0$, within the time scale of the experiment because the larger the value of $\lambda$, the longer it will take to the sample to return to its original structure. Notice that the value of $\eta$ at the end of the cycle decreases substantially as $\lambda$ increases and that the curves of viscosity versus time (inset in Fig. 12) become more asymmetrical as $\lambda$ becomes larger. These patterns have been observed in fast reforming systems (elongated micellar solutions of CTAT), which exhibit the behavior shown in the curves a and b in Fig. 12, and in slow structure-reforming systems (Aerosol OT or DDAB lamellar liquid crystalline dispersions), which behaves more like curves c and d in Fig. 11 [6,7,23].

Fig. 13 depicts the effect of applying consecutive stress cycles on the extent of thixotropy. For a sample with a small value of $\lambda$ (fast structural recovery), the areas of the thixotropic loop in the first, second and third cycles are very similar (Fig. 13(a)). In fact, the viscosity responses are alike in the three loops (inset in Fig. 13a). However, for a material with a large value of $\lambda$, the area of thixotropy after the first cycle (curve I in Fig. 13(b)) decreases substantially after the second cycle (curve II in Fig. 13(b)) and even more when the third consecutive cycle is applied (curve III in Fig. 13(b)). Moreover, the final viscosity of the material at the end of the cycle is more than two orders of magnitude lower than the initial viscosity. The reason for this behavior

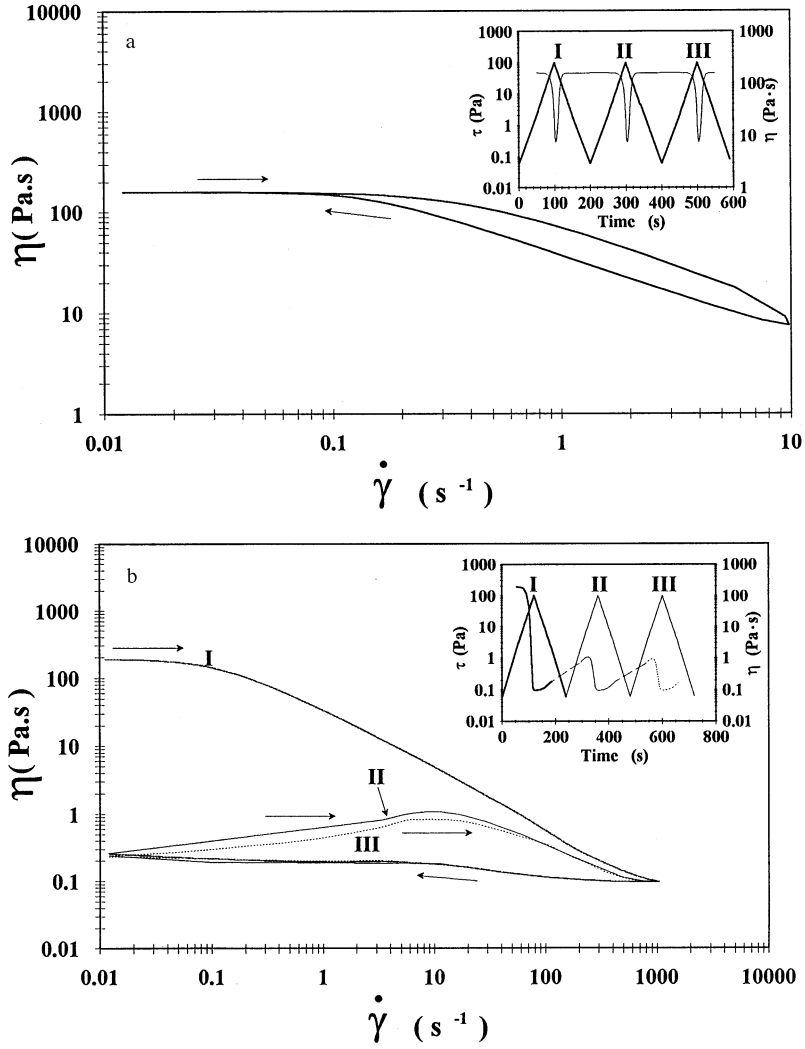


Fig. 13. Shear viscosity as a function of shear rate for three consecutive exponentially increasing and decreasing stress cycles applied on samples with different value of $\lambda$: (a) 2 s: (b) 50 s. Initial stress ($\tau_0 = 0.1$ Pa), final stress ($\tau_f = 100$) and $a(= \mathrm{d\ In}\ \tau/\mathrm{d}t) = 0.028$ are the same in all cycles. The parameters used are the same as in Fig. 3, with the exception of $\lambda$. Inset: Stress program applied and time response of viscosity.

is that with slow recovering materials (large $\lambda$), the time scale of the experiment is much shorter that the time scale for structure built up. This means that at the end of the first cycle, the material has not yet recovered its original structure, and so, the application of a second and third stress cycles destroys even more structure and the loops shrink. With fast recovering materials, this behavior does not happen because the time scale of the experiment is similar or larger than the time scale for reconstruction of structure. These two behaviors have been observed in aqueous dispersions of liquid crystals and in micellar solutions [6,7].

To demonstrate that the parameter $\lambda$ is indeed a characteristic time for structure reconstruction, a sample was subjected to a stress cycle; then it was allowed to rest for a certain period of

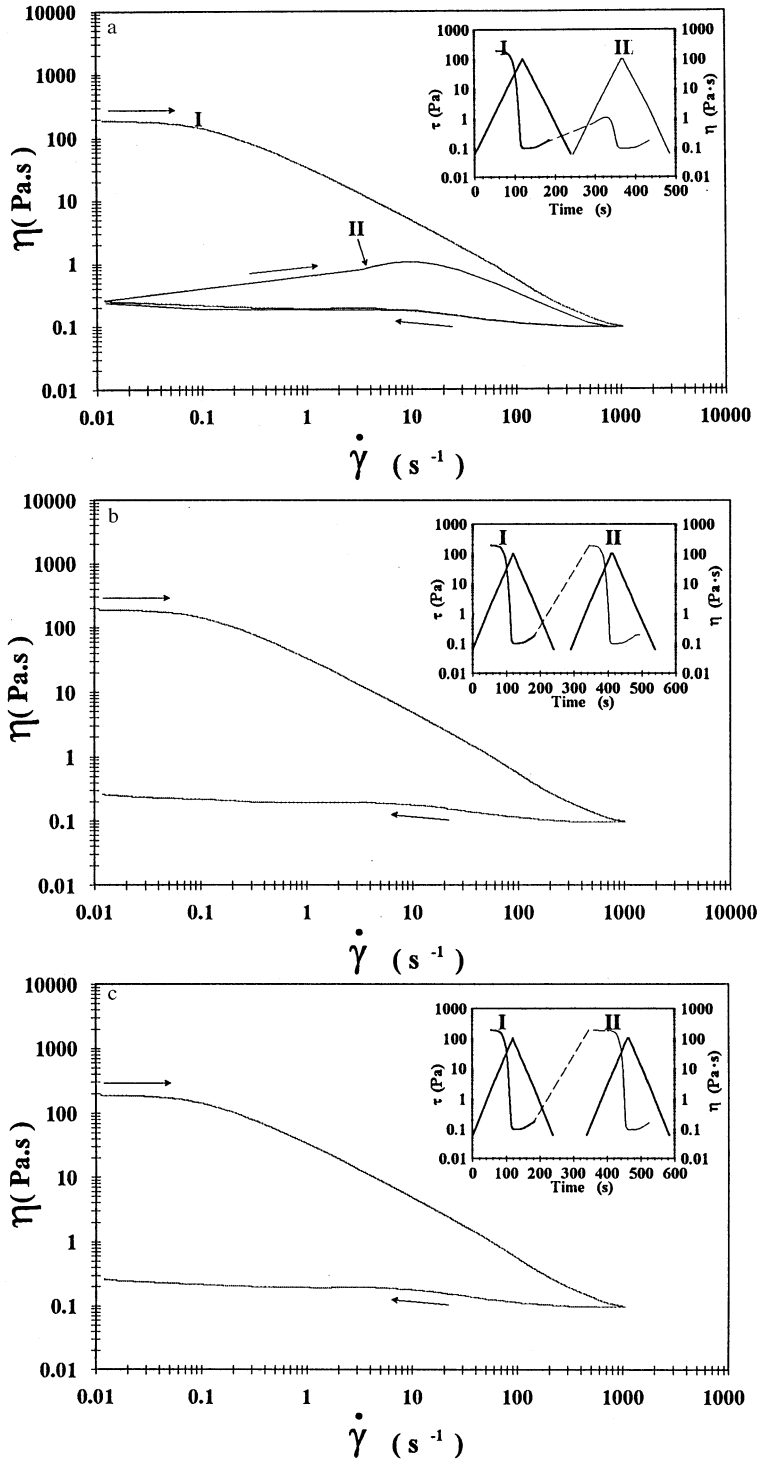


Fig. 14. Shear viscosity as a function of shear rate for exponentially increasing and decreasing stress cycles with a resting period between them: (a) 5 s; (b) 50 s; (c) 100 s. Initial stress ($\tau_0 = 0.1$ Pa), final stress ($\tau_f = 100$) and $a(= \mathrm{d} \ln \tau/\mathrm{d}t) = 0.028$ are the same in all cycles. The parameters used are the same as in Fig. 3, with the exception of $\lambda$ ($\equiv 50$ s). Inset: Stress program applied and time response of viscosity.

time before a second cycle was applied. The simulations were performed with a slow recovery material (large $\lambda$) and with resting times smaller, similar and larger than the value of $\lambda$. Upon application of the first cycle, a large hysteresis loop forms and the viscosity at the end of the cycle is almost three orders of magnitude smaller than $\eta_0$ (Fig. 14(a)). As discussed above, this is due to the fact that the material cannot recover its initial structure within the time scale of the experiment. When the rest period is smaller than $\lambda$, the thixotropic loop decreases substantially after the application of the second stress cycle—but the area is larger than when there is no rest period between the loops (curves II in Fig. 13(b) and Fig. 14(a)). As the resting time increases, the area of the thixotropic loop after the second cycle increases and resembles more the loop obtained after the first cycle. When the resting time is of the order of (Fig. 14(b)) or larger than $\lambda$ (Fig. 14(c)), the area after the first and second cycles are identical, because the material has had enough time to recover completely and to return to its equilibrium (no flow) structure before the application of the second cycle.

## 3. Conclusions

A simple model consisting of the Upper Convected Maxwell constitutive equation and a kinetic equation for destruction and construction of structure—the latter first proposed by Fredrickson [20]—is used here to reproduce the complex rheological behavior of viscoelastic micellar solutions and liquid crystalline dispersions that also exhibit thixotropy and rheopexy under shear flow. The model requires five parameters that have physical significance and that can be estimated from rheological measurements. The parameters are the Newtonian fluidity ($\varphi_0$), the high shear rate fluidity ($\varphi_\infty$), a structure dependent relaxation time ($\delta$), a characteristic time for structure built up ($\lambda$) and a kinetic constant for destruction of structure ($k$).

Several steady and unsteady shear flow situations (simple steady shear flow, stress relaxation after cessation of steady flow, creep, instantaneous stress relaxation and exponentially increasing-and decreasing stress cycles) were examined with the model. In particular, the model predicts creep behavior and the presence of thixotropic loops when the sample is subjected to transient stress cycles. Such behavior has been observed with surfactant-based viscoelastic micellar solutions, dispersions and liquid crystalline phases [6,7]. The role of the characteristic time for structure built up, $\lambda$, in the extent and shape of the thixotropic loops was demonstrated.

The merits of the model will be demonstrated in a forthcoming publication, where the predictions are compared with rheological data of viscoelastic worm-like micellar solutions, dispersions of lamellar liquid crystals and bentonite suspensions [27].

## Acknowledgements

This project was sponsored by the National Council of Science and Technology of Mexico (CONACYT grant 3397-E9309). F. Bautista recognizes the support of CONACYT.

## References


[1] K.M. Baezly, Rheometry. Industrial Applications, Research Studies Press, chap 7, 1980.
[2] A.B. Metzner, J. Rheol. 29 (1985) 739.
[3] A.M. Ait-Kadi, A. Grmela, P.J. Carreau, Rheol. Acta 27 (1988) 241.
[4] H.A. Barnes, Shear thickening in suspensions of non-aggregating solid particles dispersed in Newtonian liquids, J. Rheol. 33 (1989) 329; Thixotropy—A review, J. Non Newtonian Fluid Mech. 70 (1997) 1.
[5] A.N. Mujumdar, Rheology and fiber orientation during injection molding of ceramic suspensions, Ph.D. Thesis, University of Delaware, 1993.
[6] J.F.A. Soltero, Relacíon entre Estructura y Propiedades Reológicas de Cristales Líquidos Liòtrópicos y Poliméricos, Tesis Doctoral, U.N.A.M., México, 1995.
[7] J.F.A. Soltero, O. Robles-Vasquez, J.E. Puig, O. Manero, Thixotropic–antithixotropic behavior of surfactant-based lamellar liquid crystals under shear flows, J. Rheol 39 (1995) 235.
[8] J. F. A. Soltero, J.E. Puig, O. Manero, P.C. Schulz, Rheology of cetyltrimethyl ammonium tosilate/water system. I. Relation to phase behavior, Langmuir 11 (1995) 3337.
[9] J.F.A. Soltero, J.E. Puig, O. Manero, Rheology of cetyltrimethylammonium tosilate/water system. II. Linear viscoelastic regime, Langmair 12 (1996) 2654.
[10] J.F.A. Soltero, J.E. Puig, O. Manero, Rheology of cetyltrimethylammonium tosilate/water system. III. Non linear viscoelastic behavior, Langmuir (submitted).
[11] W.H. Bauer, E.A. Collins, Rheology. Theory and applications, vol. 4, chap. 8, Academic Press, New York, 1967, pp. 423–459.
[12] M.J. Groves, A.B. Ahmad, Rheol. Acta 156 (1976) 501.
[13] J. Mewis, Thixotropy—a general review, J. Non-Newtonian Fluid Mechs. 6 (1979) 1.
[14] H.T. Kim, R.S. Brodkey, A kinetic approach for polymer solution data, AIChE J. 14 (1968) 61.
[15] D.C.H. Cheng, F. Evans, Phenomenological characterization of the rheological behavior of inelastic reversible thixotropic an antithixotropic fluids, J. Appl. Phys. 16 (1965) 1599.
[16] D.C.H. Cheng, On the behaviour of thixotropic fluids with a distribution of structure, J. Phys. D: Appl. Phys. 7 (1974) 155.
[17] T.Y. Liu, D.S. Soong, A model for structured fluids, Chem. Eng. Commun. 22 (1983) 273.
[18] J.D. Goddard, Dissipative materials as models of thixotropy and plasticity, J. Non-Newtonian Fluid Mechs. 14 (1984) 141.
[19] D. De Kee, C.F. Chan Man Fong, Rheological properties of structured fluids, Polym. Eng. Sci. 34 (1994) 438.
[20] A.G. Fredrickson, A model for the thixotropy of suspensions, AIChE J. 16 (1970) 436.
[21] J.G. Oldroyd, Proc. R. Soc. A200 (1950) 523.
[22] F. Bautista, Tesis Doctoral, Universidad de Guadalajara, Mexico (in progress).
[23] T. Lauger, R. Linemann, W. Richtering, Shear orientation of a lamellar lyotropic liquid crystal, Rheol. Acta 34 (1995) 132.
[24] J. Ferry, Viscoelastic Properties of Polymers, Wiley, New York, 1980.
[25] M.H. Wagner, Analysis of time-dependent non-linear stress-growth data for shear and elongation flow of a low-density branched polyethylene melt, Rheol Acta 15 (1976) 136.
[26] H.M. Laun, Description of the non-linear shear behavior of a low density polyethylene melt by means of an experimentally determined strain dependent memory function, Rheol. Acta 17 (1978) 1.
[27] F. Bautista, J.F.A. Soltero, J.E. Puig, O. Manero, Understanding thixotropic and antithixotropic behavior of viscoelastic micellar solutions and liquid crystalline dispersions. II, comparison with experimental data, J. Non Newtonian Fluid Mech., 1998 (to be submitted).